

Copyright © 1997, by the author(s).  
All rights reserved.

Permission to make digital or hard copies of all or part of this work for personal or classroom use is granted without fee provided that copies are not made or distributed for profit or commercial advantage and that copies bear this notice and the full citation on the first page. To copy otherwise, to republish, to post on servers or to redistribute to lists, requires prior specific permission.

**ON SMOOTHING OF THE I-V LANGMUIR  
PROBE CHARACTERISTIC**

by

J. T. Gudmundsson

Memorandum No. UCB/ERL M97/38

3 June 1997

**ON SMOOTHING OF THE I-V LANGMUIR  
PROBE CHARACTERISTIC**

by

J. T. Gudmundsson

Memorandum No. UCB/ERL M97/38

3 June 1997

**ELECTRONICS RESEARCH LABORATORY**

College of Engineering  
University of California, Berkeley  
94720

# On Smoothing of the I-V Langmuir Probe Characteristic

J. T. Gudmundsson

Plasma Assisted Materials Processing Laboratory  
Department of Electrical Engineering and Computer Sciences  
University of California  
Berkeley, CA 94720

## Abstract

Numerical methods for noise suppression of Langmuir probe  $I - V$  characteristics are essential when numerically calculating the electron energy distribution function. We examine the use of Gaussian and Blackman windows and the distortion they introduce into the electron energy distribution function and suggest a method to determine the correct electron density and temperature from noisy  $I - V$  characteristic. The digital filter is applied to Ar/O<sub>2</sub> plasma.

## 1 Introduction

Langmuir probes are important diagnostic devices in low pressure weakly ionized plasmas. In their simplest form they are only a bare wire introduced into the plasma. They make it possible to determine the electron density  $n_e$ , the electron temperature  $T_e$ , the dc plasma potential  $V_{pl}$  and the electron energy spectrum. A number of reviews on the use of Langmuir probes to characterize plasma exist in the literature [1, 2, 3].

The floating potential is the potential (with respect to the chamber ground) at which the probe draws equal ion and electron currents (no net current). The potential at which the plasma and probe potentials are equal is referred to as the plasma potential. These two potentials divide the  $I - V$  characteristic measured by a Langmuir probe into three regions. For a highly negative applied probe voltage, all electrons are repelled and only positive ions are attracted and collected by the probe. This is called the ion saturation region. In the intermediate region some electrons are attracted to the probe as well as ions. In the electron saturation region, the probe is positive with respect to the plasma potential; the ions are fully repelled and only

electrons are collected by the probe. The second derivative of the probe  $I - V$  characteristic is proportional to the electron energy spectrum of the plasma [4] and thus it is important that it is accurately determined. Plasmas by themselves are a significant source of noise and this noise is amplified by the differentiation process. Several methods have been developed to obtain the second derivative of a measured  $I - V$  probe characteristic numerically. Fujita and Yamazaki [5] as well as Sudit and Woods [6] use a smoothing differentiation method based on the Savitzky and Golay filters. Kimura et al. [7] use a finite impulse response filter that gives the second derivative via convolution. Fernández Palop et al. [8] proposes the use of a Gaussian function as a filter. We investigate the distortion in the second derivative of the  $I - V$  probe characteristic introduced by smoothing of the data with a Gaussian and Blackman window [9]. We suggest a method to correct for the distortion and demonstrate the use of a Blackman filter and the correction method on Ar/O<sub>2</sub> plasma in a planar inductive discharge.

## 2 Experimental Apparatus

Planar inductive discharge were used to create high density plasma. High plasma density is achieved when the discharge is operated in the electromagnetic mode, in which the rf coil current induces a magnetic field that again induces an azimuthal electric field within the plasma that maintains the discharge.

The plasma chamber consists of an anodized aluminum cylinder with inner diameter 30.48 cm and length of 1 m. Movable aluminum pistons are at both ends. An aluminum electrode, 27 cm in diameter is mounted on one of these pistons. The electrode serves as a wafer holder and can be water cooled. A 2.5 cm thick by 25 cm diameter quartz plate mounted on the other piston separates the planar spiral induction coil from the plasma. Figure 1 shows a schematic of the planar inductive plasma source. The distance  $L$  between quartz plate and the wafer holder can be varied. In all the experiments described the plasma is created inside a cylindrical vacuum chamber of radius  $R = 15.24$  cm and adjusted such that the length is fixed at  $L = 7.62$  cm and the diagnostic ports are in the center plane of the chamber. The plasma chamber is evacuated by a Leybold Turbovac 361C turbomolecular pump which has a pumping speed 340 - 400 l/s backed by a W.M. Welch rotary pump giving a base pressure of about  $3 - 9 \times 10^{-6}$  Torr. The equilibrium gas pressure in the chamber is monitored with an MKS Baratron capacitance manometer model 127 connected to a MKS Type PDR-C-2C Power Supply Digital Readout. To further control the chamber pressure the gate valve was manually adjusted to vary the pumping speed. The pressure can be varied in the range 0.5 - 300 mTorr. The source is powered at 13.56 MHz using a 1 kW Henry 1000D Radio Frequency Power Generator connected to an L-type capacitive matching network. The power supply operates in the range 0 - 1000 W. For all measurements the aluminum plasma chamber, electrodes and pistons are grounded.

A cylindrical Langmuir probe with a separate reference electrode is used in the experiment. The probe system is similar to that described by Godyak et al. [3].

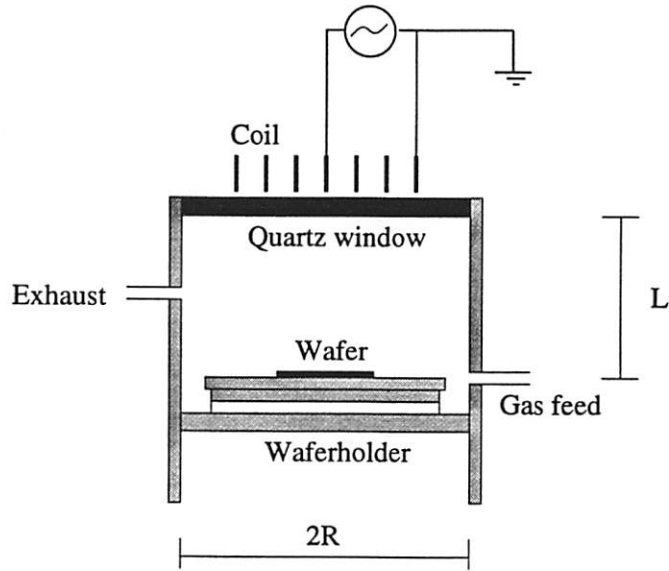


Figure 1: A schematic of the planar inductive discharge.

A small measurement probe is surrounded by a wire loop reference probe. Both probes are introduced into the center of the discharge chamber. A sawtooth voltage measuring technique is applied to measure the probe characteristics. The applied probe voltage is swept linearly in time for short duration and the probe current is measured. The sweeping time can be varied in the range 0.2 – 5 ms and the voltage sweep can be varied in the range 2 – 50 V. A sweeping time of a few milliseconds or less is selected to keep the probe temperature constant to avoid changes in its work function during a sweep [3]. The probe current  $I_{pr}$  is measured by sensing the voltage across a resistor. The current sensor resistor can be varied in the range 0 – 20 k $\Omega$ . To avoid probe contamination a continuous probe cleaning is performed by ion bombardment. This is done by applying a high negative voltage pulse (30 – 60 V) in the time interval between ramp pulses of the voltage sweep. The probe voltage and the probe current from the probe driving circuit and the trigger signal to the driving circuit, from the computer, are fed into a shielded I/O connector box, National Instruments model SCB-100 and from there the measured values are read into a computer via AT-MIO-64E-3 data acquisition card from National Instruments. The probe current and voltage are read into a 12-bit A/D converter on the data acquisition card. The  $I - V$  data consist usually of roughly 512 or 1024 points. The  $I - V$  curve can be averaged as needed to improve the signal-to-noise ratio. The measurement is then repeated a desired number of times and an average curve is calculated. For all the measurements presented here the  $I - V$  curve was averaged 1000 times. The Langmuir probe construction is shown in figure 2. The measurement probe is a cylindrical tungsten rod  $l_{pr} = 4.0$  mm in length and  $r_{pr} = 63.5$   $\mu$ m in radius. A probe holder  $l_{prh} = 11$  mm long and  $r_{prh} = 0.5$  mm in radius is next to the probe tip. The reference probe is a wire loop 2 cm in radius made of 0.5 mm diameter

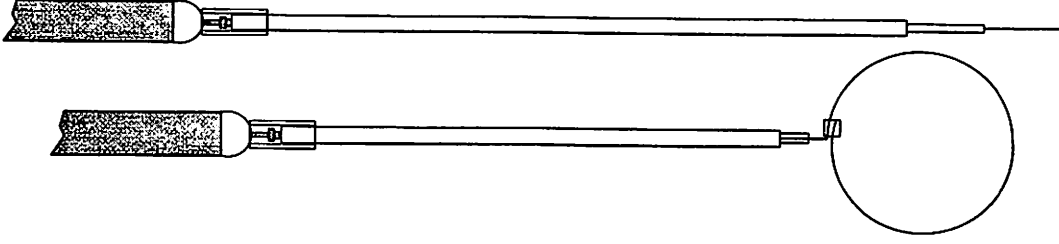


Figure 2: The Langmuir probe. The probe tip length is  $l_{pr} = 4.0$  mm long and its radius  $r_{pr} = 63.5$   $\mu\text{m}$ . The probe holder is  $l_{prh} = 11$  mm long and its radius  $r_{prh} = 0.5$  mm. The reference probe is a wire loop 2 cm in diameter made of 0.5 mm diameter tungsten wire.

tungsten wire also shown in figure 2. The reference loop is not closed and the ring structure is kept by an insulating holder. Both probes are supported by 0.5 mm diameter tungsten rods covered fixed by insulating tubes 2 mm in diameter and 112 mm long for the measurement probe and 82 mm long for the reference probe.

### 3 Electron Energy Distribution Function

The classical Langmuir approach is applied to the electron collection region of the probe characteristics where the probe potential is less than the plasma potential. From the measured probe current the first derivative is calculated numerically and the plasma potential is found from the maximum of the first derivative. The electron temperature  $T_e$  is calculated from the slope of the line that fits  $\ln I_e$  versus  $V$  and the electron saturation current is defined as

$$I_{esat} = \frac{1}{4} e n_L \bar{v}_e A_{pr} \quad (1)$$

where the probe voltage equals the plasma potential,  $A_{pr} = 2\pi l_{pr} r_{pr}$  is the area of the measurement probe,  $\bar{v}_e = (8eT_e/\pi m_e)^{1/2}$  is the mean electron speed and  $n_L$  is the plasma density in the probe neighborhood. Note that when the probe voltage  $V$  equals the plasma potential  $V_{pl}$  there is no sheath.

A relation between the second derivative of the  $I - V$  characteristics and the electron energy distribution function was discussed by Mott-Smith and Langmuir [10], and Druyvesteyn [4] showed that the second derivative of the probe current with respect to the probe bias voltage is proportional to the electron energy distribution function  $g_e(V)$ . The electron energy distribution function (EEDF) is given as [11]

$$g_e(V) = \frac{2m}{e^2 A_{pr}} \left( \frac{2eV}{m} \right)^{1/2} \frac{d^2 I_e}{dV^2} \quad (2)$$

which is referred to as the Druyvesteyn formula. The electron energy probability function (EPPF) is given by

$$g_p(\mathcal{E}) = \mathcal{E}^{-1/2} g_e(\mathcal{E}) \quad (3)$$

where  $\mathcal{E}$  is the electron energy. The plasma potential is the voltage where the second derivative of the electron current  $I_e$  is zero.

The electron density  $n_e$  is determined by

$$n_e = \int_0^{\infty} g_e(\mathcal{E})d\mathcal{E} \quad (4)$$

and the average energy, by

$$\langle \mathcal{E}_e \rangle = \frac{1}{n_e} \int_0^{\infty} \mathcal{E}g_e(\mathcal{E})d\mathcal{E} \quad (5)$$

which gives the effective electron temperature as

$$T_{eff} = \frac{2}{3}\langle \mathcal{E}_e \rangle \quad (6)$$

## 4 Smoothing Methods

Digital filters were tested by a numerical simulation of the Langmuir probe  $I - V$  characteristic. For simplicity the electron energy distribution is assumed to be Maxwellian. The cylindrical probe collects electron current of the form

$$I(V) = \begin{cases} I_o \exp\left(\frac{V-V_{pl}}{T_e}\right) & \text{if } V - V_{pl} < 0 \\ I_o \left(1 + \frac{V-V_{pl}}{T_e}\right)^{1/2} & \text{if } V - V_{pl} \geq 0 \end{cases} \quad (7)$$

The numerical simulation is performed for  $I_o = 2$  mA and the electron temperature is set to  $T_e = 2.0$  eV and  $V_{pl} = 12$  V. We assume  $r_{pr} = 63.5 \mu\text{m}$  and  $l_{pr} = 5$  mm. This corresponds to an electron density of  $2.51 \times 10^{16} \text{ m}^{-3}$ . The noise is added to the collected current by adding a function  $n(V) = 0.01 \times (-1)^k R I_o$  where  $k = 0, 1, 2, \dots$  and  $R$  is a vector of random numbers with uniform distribution on the interval  $[0.0, 1.0]$ . We assume the probe voltage  $V$  to be in the range  $-30 - 20$  V, equally divided to give 1001 points, with a sweep time of 5 ms. The sampling frequency is thus  $f_s = 200.2$  kHz.

The resulting current  $I(V) + n(V)$  is then fed into a discrete time filter. The convolution sum relating the input and output of a discrete time filter is given as

$$y(n) = \sum_{k=-\infty}^{\infty} x(k)w(n-k) \quad (8)$$

where  $w(n)$  is the system function of the discrete filter. The second derivative of the filtered signal is then found by applying central difference approximation twice on the  $I - V$  characteristic. The output of the filter is compared to the unfiltered noiseless input signal. Applying the smoothing to the  $I - V$  probe characteristic introduces distortion in the electron energy probability function, in particular at low electron energy. The effect of the distortion introduced by the smoothing on the plasma parameters for different degree of smoothing is compared for two filters, Gaussian and

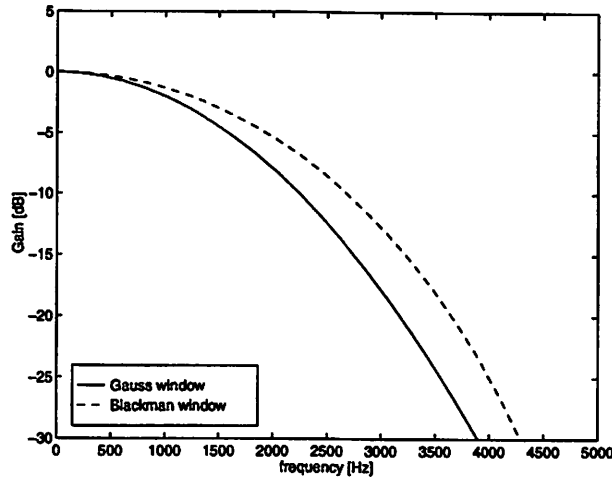


Figure 3: The frequency response of the Gaussian ( $\sigma = 1.1$ ) and Blackman ( $M = 112$ ) windows. The cutoff frequency is  $\omega_c = 1231.4$  Hz and  $\omega_c = 1510.9$  Hz for the Gaussian window and the Blackman window respectively.

Blackman windows. The distortion leads to underestimation of the electron density and overestimation of the effective electron temperature. The frequency response for Gaussian and Blackman windows is shown in figure 3.

As suggested by Rundle et al. [12] the measured electron energy distribution function can be fitted to the function

$$g_R(E) = a\sqrt{E} \exp(-bE^x) \quad (9)$$

where  $a$ ,  $b$  and  $x$  are constants. The Maxwellian electron energy distribution is a special case of equation (9) with  $x = 1$  and the Druyvesteyn distribution is a special case with  $x = 2$ . The value of  $x$  was determined by performing a least-squares analysis of  $\ln(g_R(E)/\sqrt{E})$  versus  $E^x$  for various  $x$  to find the best fit. The maximum of the electron energy distribution function is found and the corresponding electron energy. Equation (9) is fitted to the measured electron energy distribution function from the electron energy where the electron energy distribution function has maximum value until it has fallen two orders of magnitude. The best fit to equation (9) is then interpolated to zero electron energy, and the electron density and effective electron temperature calculated, referred to as  $n_e^{corr}$  and  $T_{eff}^{corr}$  in tables 1, 2, 3 and 4.

#### 4.1 Gaussian Window

Hyden [13] introduced a simple iterative data smoothing algorithm that utilizes a Gaussian distribution function as a filter. Fernández Palop et al. [8] apply this filter to smooth the Langmuir probe  $I - V$  characteristic. The Gaussian filter is given as

$$w_G(x) = \sum_{k=1}^n \binom{n}{k} (-1)^{k+1} \frac{1}{\sigma\sqrt{2\pi k}} \exp\left(\frac{-x^2}{2\sigma k^2}\right) \quad (10)$$

Table 1: Plasma parameters evaluated for different filter parameters using a Gaussian filter.

$\sigma$	$V_{pl}$ [V]	$T_e$ [eV]	$T_{eff}$ [eV]	$T_{eff}^{corr}$ [eV]	$n_L$ [m <sup>-3</sup> ]	$n_e$ [m <sup>-3</sup> ]	$n_e^{corr}$ [m <sup>-3</sup> ]
0	11.90	2.0000	2.0061	2.0061	$2.51 \times 10^{16}$	$2.51 \times 10^{16}$	$2.51 \times 10^{16}$
0.2	11.70	2.0000	2.0271	2.0061	$2.28 \times 10^{16}$	$2.26 \times 10^{16}$	$2.28 \times 10^{16}$
1.1	11.60	2.0141	2.4442	2.0563	$2.17 \times 10^{16}$	$1.91 \times 10^{16}$	$2.36 \times 10^{16}$
1.5	11.75	2.0528	2.7477	2.1394	$2.25 \times 10^{16}$	$1.87 \times 10^{16}$	$2.60 \times 10^{16}$

where  $n$  is the number of iterations and  $\sigma$  is the standard deviation. The number of iterations is chosen to be equal to one and the standard derivation is varied to determine the degree of smoothing.

Table 1 and figure 4 (a) show the results of applying a Gaussian filter to a noiseless numerically simulated  $I-V$  probe characteristic. In the table  $T_e$  refers to the electron temperature calculated from the slope of  $\ln I_e$  versus  $V$ ,  $T_{eff}$  is found by integrating over the measured electron energy distribution function and  $T_{eff}^{corr}$  is found by integrating over a fit to the electron energy distribution function interpolated down to low electron energies. Similarly  $n_L$  is calculated applying Langmuir's method (equation (1)),  $n_e$  is found by integrating over the measured electron energy distribution function and  $n_e^{corr}$  is found by integrating over a fit to the electron energy distribution function interpolated down to low electron energies. The smoothing distorts the electron energy probability functions and leads to overestimation of the effective electron temperature and underestimation of the electron density. Table 2 and figure 4 (b) show the effect of the degree of smoothing on the noisy  $I-V$  probe characteristic using a Gaussian window. We note that to achieve acceptable signal to noise ratio in the second derivative the low energy part of the electron energy probability function is seriously distorted. This leads to overestimation of the effective electron temperature and underestimation of the electron density. For the assumed numerical  $I-V$  probe characteristic  $\sigma = 1.1$  gives the optimum trade off between noise suppression and distortion due to smoothing. We fit equation (9) to the electron energy distribution function from its maximum value. The fitted electron electron energy distribution is then interpolated to lower electron energies to recover the electron temperature and electron density within few percent. It is interesting to note that Langmuir's method gives a good estimate of the electron temperature and density regardless of noise added and degree of smoothing over the range of parameters investigated.

## 4.2 Blackman Window

The Blackman window is given as [9]

$$w_B(n) = 0.42 - 0.5 \cos \frac{2\pi n}{M} + 0.08 \cos \frac{4\pi n}{M}, \quad n = 0, 1, 2, \dots, M. \quad (11)$$

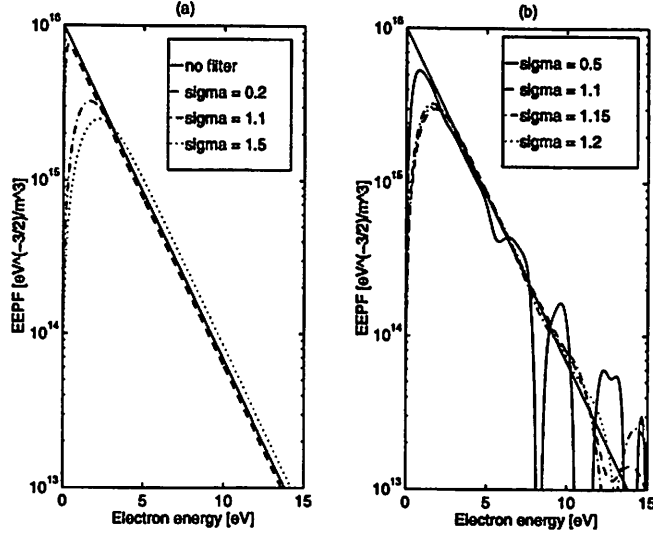


Figure 4: The electron energy probability function (EPPF) versus the electron energy for numerically simulated  $I - V$  Langmuir probe characteristics. (a) Unfiltered signal is compared to signal smoothed by a Gaussian window with  $\sigma = 0.2, 1.1$  and  $1.5$ . (b) Noisy signal filtered by a Gaussian window with  $\sigma = 0.5, 1.1, 1.15$  and  $1.2$ .

Table 2: Plasma parameters evaluated for different filter parameters using a Gaussian window, with added noise.

$\sigma$	$V_{pl}$ [V]	$T_e$ [eV]	$T_{eff}$ [eV]	$T_{eff}^{corr}$ [eV]	$n_L$ [m <sup>-3</sup> ]	$n_e$ [m <sup>-3</sup> ]	$n_e^{corr}$ [m <sup>-3</sup> ]
0.2	11.70	2.0188	2.1985	7.0719	$2.33 \times 10^{16}$	$2.33 \times 10^{16}$	$5.30 \times 10^{16}$
0.5	11.60	1.9905	2.1736	1.7152	$2.19 \times 10^{16}$	$2.09 \times 10^{16}$	$5.76 \times 10^{16}$
0.9	11.60	2.0082	2.3711	1.6106	$2.17 \times 10^{16}$	$1.97 \times 10^{16}$	$3.58 \times 10^{16}$
1.0	11.60	2.0184	2.3578	2.1372	$2.16 \times 10^{16}$	$1.93 \times 10^{16}$	$2.17 \times 10^{16}$
1.1	11.60	2.0290	2.4217	2.0817	$2.16 \times 10^{16}$	$1.91 \times 10^{16}$	$2.35 \times 10^{16}$
1.15	11.65	2.0152	2.4801	2.1275	$2.20 \times 10^{16}$	$1.92 \times 10^{16}$	$2.36 \times 10^{16}$
1.2	11.65	2.0202	2.5504	2.1572	$2.20 \times 10^{16}$	$1.91 \times 10^{16}$	$2.34 \times 10^{16}$
1.4	11.75	2.0203	2.6921	2.2405	$2.24 \times 10^{16}$	$1.88 \times 10^{16}$	$2.40 \times 10^{16}$

Table 3: Plasma parameters evaluated for different filter parameters using a Blackman window.

$M$	$V_{pl}$ [V]	$T_e$ [eV]	$T_{eff}$ [eV]	$T_{eff}^{corr}$ [eV]	$n_L$ [m <sup>-3</sup> ]	$n_e$ [m <sup>-3</sup> ]	$n_e^{corr}$ [m <sup>-3</sup> ]
50	11.575	2.0000	2.0660	2.0062	$2.16 \times 10^{16}$	$2.10 \times 10^{16}$	$2.17 \times 10^{16}$
110	11.575	2.0041	2.3141	2.0497	$2.15 \times 10^{16}$	$1.95 \times 10^{16}$	$2.25 \times 10^{16}$
112	11.575	2.0045	2.3229	2.0488	$2.17 \times 10^{16}$	$1.95 \times 10^{16}$	$2.26 \times 10^{16}$
120	11.575	2.0062	2.3587	2.0286	$2.15 \times 10^{16}$	$1.93 \times 10^{16}$	$2.32 \times 10^{16}$

Table 4: Plasma parameters evaluated for different filter parameters using a Blackman window with added noise.

$M$	$V_{pl}$ [V]	$T_e$ [eV]	$T_{eff}$ [eV]	$T_{eff}^{corr}$ [eV]	$n_L$ [m <sup>-3</sup> ]	$n_e$ [m <sup>-3</sup> ]	$n_e^{corr}$ [m <sup>-3</sup> ]
50	11.575	1.9972	1.8792	3.0227	$2.16 \times 10^{16}$	$2.08 \times 10^{16}$	$3.89 \times 10^{16}$
110	11.575	2.0042	2.3152	1.8763	$2.15 \times 10^{16}$	$1.95 \times 10^{16}$	$2.88 \times 10^{16}$
112	11.575	2.0080	2.3894	2.0349	$2.15 \times 10^{16}$	$1.96 \times 10^{16}$	$2.28 \times 10^{16}$
120	11.575	2.0093	2.4176	2.0476	$2.15 \times 10^{16}$	$1.94 \times 10^{16}$	$2.29 \times 10^{16}$
130	11.625	2.0204	2.3606	2.1091	$2.18 \times 10^{16}$	$1.92 \times 10^{16}$	$2.29 \times 10^{16}$

where  $M$  is the size of the window and controls the degree of smoothing. Blackman window minimizes the sidelobe level while having a steep rolloff on the sidelobe. Table 3 and figure 5 (a) show the results of applying a Blackman window to a noiseless numerically simulated  $I - V$  probe characteristic. The smoothing distorts the electron energy probability functions and leads to overestimation of the effective electron temperature and underestimation of the electron density. Table 4 and figure 5 (b) show the effect of the degree of smoothing on the noisy  $I - V$  probe characteristic using a Blackman window. For the assumed numerical  $I - V$  probe characteristic  $M = 112$  gives the optimum trade off between noise suppression and distortion due to smoothing. To recover the electron density and effective electron temperature values we apply a fit to equation (9) from the electron energy where the electron energy distribution function is maximum. The fitted electron energy distribution function is then interpolated to lower energies.

## 5 RF Suppression

In rf excited plasmas interference due to the rf voltage across the probe sheath is a well known problem [3, 14, 15, 16]. The rf interaction with the probe sheath results in distortion of the probe characteristics. Attempts to reduce rf distortion include

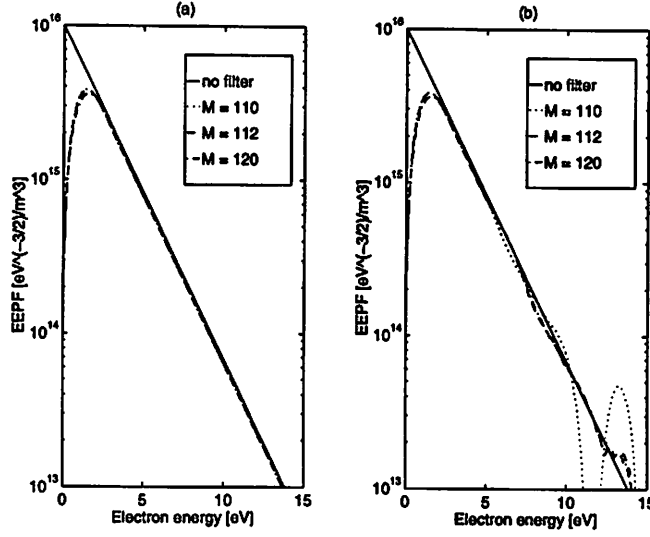


Figure 5: The electron energy probability function (EEPF) versus the electron energy for numerically simulated  $I - V$  Langmuir probe characteristics. (a) Unfiltered signal is compared to signal smoothed by a Blackman window with  $M = 110, 112$  and  $120$ . (b) Noisy signal smoothed by a Blackman window is compared for  $M = 110, 112$  and  $120$ .

introducing an inductive choke in the probe circuit to increase the rf input impedance of the probe measurement circuitry [3, 14]. Godyak et al. [2, 3, 15] give a relation between the probe plasma impedance  $Z_p$  and the probe circuit impedance  $Z_L$  that must be fulfilled for undistorted measurements in rf plasma

$$\frac{Z_p}{Z_p + Z_L} \leq 0.35 \frac{T_e}{V_{rfp}} \quad (12)$$

where  $V_{rfp}$  is the rf voltage across the probe sheath. Measurements of rf plasma potential in an inductive discharge indicate that  $V_{rfp} \approx 1 - 4$  V for argon plasma 10 - 60 mTorr and power 10 - 600 W [18].

The overall plasma impedance  $Z_p$  consists of the sheath capacitance  $C_p$  in parallel with the sheath differential resistance  $R_p$  as shown in figure 6 [14]. The sheath differential resistance is given by

$$R_p = \left( \frac{dI_{pr}}{dV_p} \right)^{-1} \approx \frac{T_e}{I_{pr}} \quad (13)$$

and has its minimum value when the probe potential is equal to the plasma potential. The sheath capacitance is estimated assuming a cylindrical capacitor where the inner radius is equal to the probe radius  $r_{pr}$  and the outer radius is the sum of the probe radius  $r_{pr}$  and the sheath thickness  $s_m$ . The sheath capacitance is thus

$$C_p \approx \frac{2\pi\epsilon_0 l_{pr}}{\ln\left(\frac{r_{pr} + s_m}{r_{pr}}\right)} \quad (14)$$

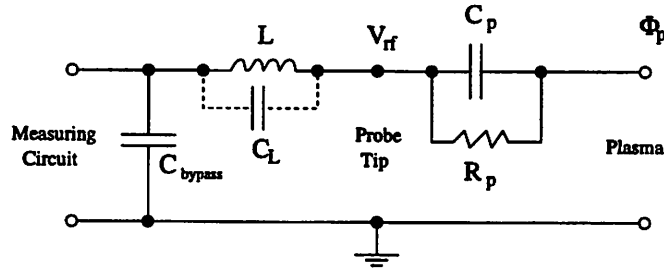


Figure 6: The equivalent circuit of the probe circuit and the rf choke.

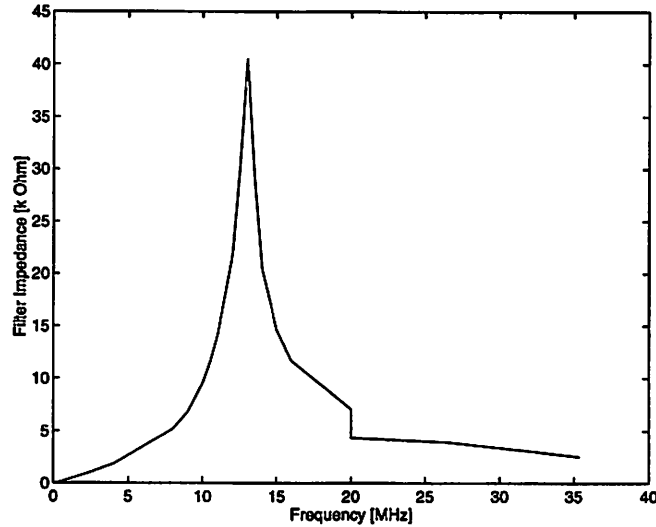


Figure 7: The probe rf filter impedance versus frequency.

where  $l_{pr}$  is the probe length and  $s_m \approx 2.612\lambda_D$  for  $V_{sh} < 5T_e$  [19], where  $V_{sh}$  is the fundamental rf voltage amplitude across the sheath and  $\lambda_D = (\epsilon_0 T_e / en_e)^{1/2}$  is the Debye length. We assume a probe of length  $l_{pr} = 7.5$  mm and radius  $r_{pr} = 63.5$   $\mu\text{m}$ . If  $T_e = 3$  eV and  $n_e = 2 \times 10^{16}$   $\text{m}^{-3}$  we find  $s_m = 2.37 \times 10^{-4}$  m and for  $n_e = 2 \times 10^{18}$   $\text{m}^{-3}$  we find  $s_m = 2.37 \times 10^{-5}$  m. This corresponds to  $C_p \approx 0.3$  pF and 1.3 pF and  $Z_p$  of 48.8 k  $\Omega$  and 8.9 k $\Omega$  respectively in the worst case when  $R_p$  is large.

The rf filter consists of a 82  $\mu\text{H}$  inductive choke in series with the measurement probe. The filter impedance versus frequency is shown in figure 7. The resonance at 13.5 MHz corresponds to  $Z_L \approx 40$  k $\Omega$  impedance. Equation (12) is thus fulfilled in a planar inductive discharge for  $n_e > 2 \times 10^{10}$   $\text{m}^{-3}$ .

## 6 Experimental Results

To demonstrate the digital filtering method Ar/O<sub>2</sub> plasma at 15 mTorr and 250 W is investigated. By varying the Ar/O<sub>2</sub> ratio the electron density is varied from  $3.33 \times 10^{10}$   $\text{m}^{-3}$  –  $3.47 \times 10^{11}$   $\text{m}^{-3}$  and the electron temperature from 2.7 eV – 4.5 eV.

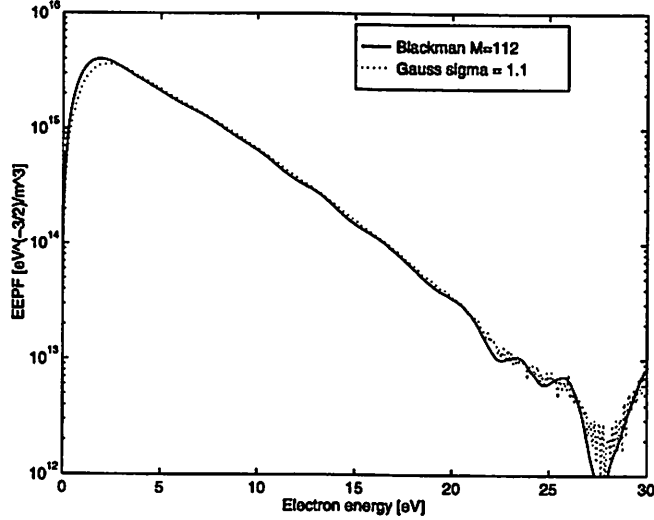


Figure 8: The electron energy probability function versus the electron energy comparing Blackman and Gauss Windows 33 % Ar/66 % O<sub>2</sub> at 15 mTorr and 249 W.

Figure 8 shows a comparison of Blackman ( $M = 112$ ) and Gauss ( $\sigma = 1.1$ ) windows for 33 % Ar/66 % O<sub>2</sub> plasma at 15 mTorr and 249 W. The two windows show similar results over the electron energy range of interest but the Blackman window introduces slightly less distortion at low electron energy and gives slightly better smoothing at high electron energy. The Blackman window is thus preferred over the Gaussian window and is used for further analysis of the data. Figure 9 shows the electron energy probability function for Ar/O<sub>2</sub> plasma at 15 mTorr and 250 W for different Ar content. As the argon content is increased the electron density increases. In table 5 the plasma parameters for different Ar/O<sub>2</sub> ratios are compared. The electron density  $n_e^{corr}$  and electron temperature  $T_{eff}^{corr}$  calculated by applying interpolation at the lowest electron energies are compared to the values calculated without applying this correction. The corrected electron temperature value is roughly 10 % lower than the distorted value. The corrected electron density is roughly 10 % higher than the value calculated using the distorted electron energy distribution function.

The effective electron temperature shown in figure 10 as well as the electron density shown in figure 11 are corrected for the distortion introduced by probe contamination or the smoothing of the  $I - V$  characteristic. The effective electron temperature and electron density are calculated by applying equation (6) and equation (4) respectively to the electron energy distribution function in equation (9) that gives the best fit to the measured data and is interpolated to low energy. Figure 10 shows the effective electron temperature  $T_{eff}$  versus the fractional argon flowrate in Ar/O<sub>2</sub> plasma at 15 mTorr and about 250 W applied power. We note that the effective electron energy is the highest for pure oxygen plasma, 4.17 eV, falls as argon content is increased, to a minimum at about 66 % Ar, and increases again to 3.3 eV for pure

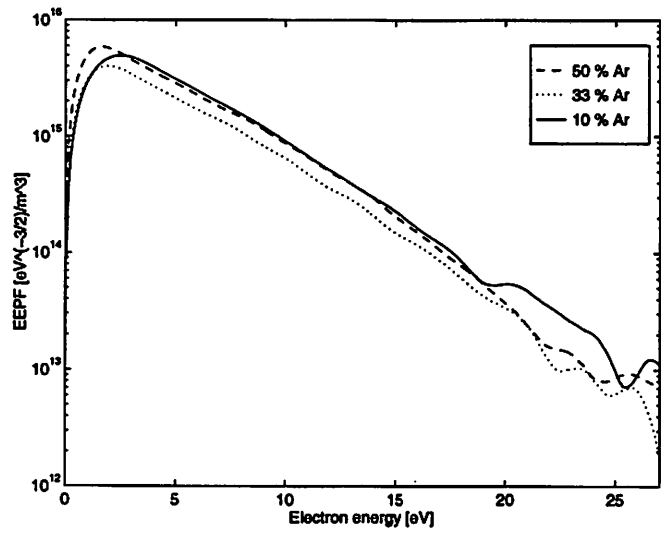


Figure 9: The electron energy probability function versus the electron energy for different Ar/O<sub>2</sub> ratios at 15 mTorr and 250 W.

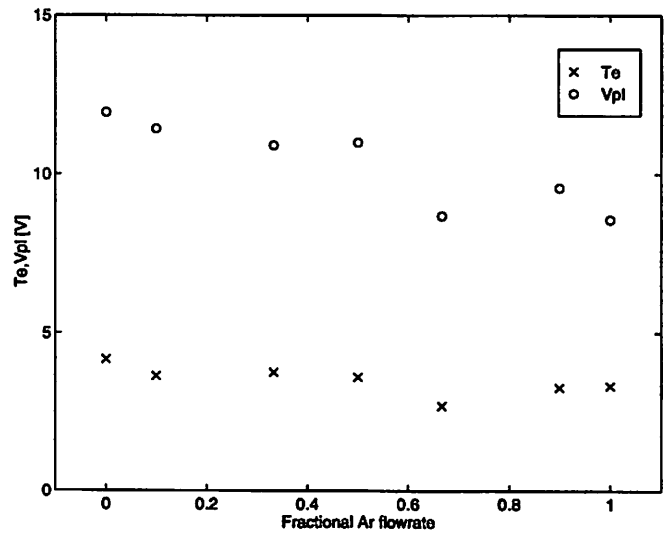


Figure 10: The electron temperature and plasma potential versus fractional argon content in Ar/O<sub>2</sub> plasma at 15 mTorr and power about 250 W.

Table 5: Plasma parameters evaluated for Ar/O<sub>2</sub> plasma.

Ar/O <sub>2</sub>	$P_{abs}$ [W]	$T_{eff}$ [eV]	$T_{eff}^{corr}$ [eV]	$n_e$ [m <sup>-3</sup> ]	$n_e^{corr}$ [m <sup>-3</sup> ]
90 %/10 %	268	3.65	3.28	$3.14 \times 10^{17}$	$3.39 \times 10^{17}$
67 %/33 %	275	3.27	2.70	$2.66 \times 10^{17}$	$2.87 \times 10^{17}$
50 %/50 %	264	4.08	3.61	$6.48 \times 10^{16}$	$7.15 \times 10^{16}$
33 %/67 %	249	4.14	3.77	$4.72 \times 10^{16}$	$5.16 \times 10^{16}$
10 %/90 %	227	4.34	3.65	$3.48 \times 10^{16}$	$4.19 \times 10^{16}$
0 %/100 %	220	4.52	4.17	$3.02 \times 10^{16}$	$3.33 \times 10^{16}$

Ar plasma. The variation in the plasma potential  $V_{pl}$  with argon content is shown in figure 10 as well. The plasma potential is the highest in pure oxygen plasma and falls as the argon content is increased. Figure 11 shows the electron density variation with the fractional argon flowrate. We note that at about 60 % Ar the electron density increases abruptly by a factor of five.

## 7 Conclusion

We demonstrate the use of Gaussian and Blackman windows to smooth the  $I - V$  Langmuir probe characteristics. The use of digital filters introduces a distortion to the electron energy distribution function in addition to the possible distortion introduced by probe contamination, rf noise and finite resistance of the plasma and electronic circuitry [2]. We suggest a method to interpolate the electron energy probability function to lower energy and recover the effective electron temperature and density values that are lost in the smoothing procedure.

The Blackman window is preferred over the Gauss window since it leads to slightly less distortion at low electron energy and better smoothing at high energy. The values of the electron density for typical plasma parameters in an actual plasma in an inductive discharge are off by 10 - 15 % due to distortion introduced by the digital smoothing and/or probe contamination. It is important to correct for this distortion to get the true values of electron density and temperature.

### Acknowledgments

This work was partially supported by NSF Grant ECS-9202993 and by a gift from the Lam Research Corporation.

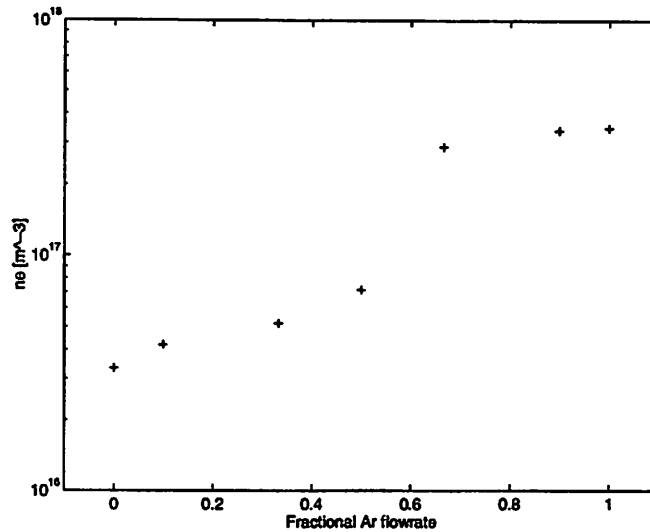


Figure 11: The electron density versus fractional argon content in Ar/O<sub>2</sub> plasma at 15 mTorr and power about 250 W.

## References

- [1] N. Hershkowitz, *How Langmuir Probes Work*, in *Plasma Diagnostics*, vol. 1, edited by O. Auciello and D.L. Flamm, Academic Press, 1989
- [2] V.A. Godyak, in, *Plasma-Surface Interaction and Processing of Materials* NATO Advanced Study Institutes, Ser. E. vol. 176, edited by O. Auciello et al, Kluwer Academic, p. 95 -134, 1990
- [3] V.A. Godyak, R.B. Piejak and B.M. Alexandrovich, *Plasma Sources Science and Technology* 1 (1992) 36 - 58
- [4] M.J. Druyvesteyn, *Zeitschrift für Physik* 64 (1930) 781 - 798
- [5] F. Fujita and H. Yamazaki, *Japanese Journal of Applied Physics* 29 (1990) 2139 - 2144
- [6] I.D. Sudit and R.C. Woods *Review of Scientific Instruments* 64 (1993) 2440 - 2448
- [7] T. Kimura, A. Yoneya and K. Ohe, *Japanese Journal of Applied Physics* 30 (1991) 1877 - 1881
- [8] J.I. Fernández Palop, J. Ballesteros, V. Colomer and M.A. Hernández, *Review of Scientific Instruments* 66 (1995) 4625 - 4636
- [9] L. B. Jackson, *Digital Filters and Signal Processing*, Kluwer Academic Publishers, 1986
- [10] H.M. Mott-Smith and I. Langmuir, *Physical Review* 28 (1926) 727 - 763

- [11] M.A. Lieberman and A.J. Lichtenberg, *Principles of Plasma Discharges and Materials Processing*, John Wiley & Sons, 1994, p. 177
- [12] H.W. Rundle, D.R. Clark and J.M. Deckers, *Canadian Journal of Physics* **51** (1973) 144 - 148
- [13] H.C. Hyden, *Computers in Physics* **1** (1987) 74 - 75
- [14] R.R.J. Gagné and A. Cantin, *Journal of Applied Physics* **43** (1972) 2639 - 2647
- [15] V.A. Godyak and O.A. Popov, *Soviet Physics - Technical Physics* **22** (1977) 461 - 464
- [16] V.A. Godyak and S.N. Oks, *Soviet Physics - Technical Physics* **24** (1979) 1255 - 1256
- [17] V.A. Godyak and R.B. Piejak, *Journal of Applied Physics* **68** (1990) 3157 - 3162
- [18] G. Gregori, *Experiments and Theoretical Models on Radio-Frequency Inductive Discharges*, Thesis, University of Bologna, Italy, 1996
- [19] V.A. Godyak and N. Sternberg, *Physical Review A* **42** (1990) 2299 - 2312